Dyes and Pigments 139 (2017) 42e49

Contents lists available at ScienceDirect

Dyes and Pigments

journal homepage: www.elsevier.com/locate/dyepig

Improving photovoltaic properties of the linear A-Ar-A type small molecules with rhodanine by extending arylene core

Bin Liu [a], Linrui Duan [a, c], Jianhua Chen [a], Xiongwei Duan [a], Ting Lei [a], Yufeng Cai [a], Qiong Wang [a], Hua Tan [a, **], Renqiang Yang [c, ***], Weiguo Zhu [a, b, *]

[a] College of Chemistry, Xiangtan University, Key Lab of Environment-Friendly Chemistry and Application in Ministry of Education, Xiangtan 411105, PR China

[b] School of Materials Science and Engineering, Jiangsu Collaborative Innovation Center of Photovoltaic Science and Engineering, Changzhou University, Changzhou 213164, PR China

[c] Qingdao Institute of Bioenergy and Bioprocess Technology, Chinese Academy of Sciences, Qingdao 266101, PR China

article info

Article history:
Received 8 October 2016
Received in revised form
8 December 2016
Accepted 8 December 2016
Available online 11 December 2016

Keywords:
A-Ar-A type small molecules
Arylene
Dicyanomethylene-rhodanine
Photovoltaic property
Organic solar cells

abstract

In order to efficiently tune photovoltaic performance, a series of linear A-Ar-A type small molecules (SMs) of $(DRCN3T)_2Ar$ were designed and synthesized, which contain the same terminal of 2-(1,1-dicyanomethylene) rhodanine (DRCN) and p-bridged space of 5-vinyl-trithiophene (3T), but different central arylene (Ar) unit, respectively. Significantly extending film absorption and increasing hole mobility were obtained in these SMs with enlarging Ar units from phenylene (Ph), naphthylene (Nap) to anthrylene (Ant). As a result, photovoltaic properties were remarkably improved in these SM/$PC_{71}BM$ based solution-processing organic solar cells (OSCs) by enlarging Ar units in $(DRCN3T)_2Ar$. The highest power conversion efficiency of 5.15% with a short-circuit current density of 11.34 mA cm^{-2} was obtained in the $(DRCN3T)_2Ant$ based device, which is three times of that in the $(DRCN3T)_2Ph$-based device. Our work further indicates that properly extending Ar core could be beneficial to improve photovoltaic properties for the A-Ar-A type SMs.

1. Introduction

Organic solar cells (OSCs) with bulk heterojunction (BHJ) architectures have been considered as a promising solar energy conversion technology because of their some advantages of solution processablility, lightweight, low-cost and flexibility in large-area applications [1e9]. Their photovoltaic performances have been rapidly improved by development of novel photovoltaic materials and optimization of device processing technology in the past few years. Much progress with a power conversion efficiency (PCE) about 10% was achieved in the single-junction polymer-based OSCs (PSCs) and small/oligomer molecule-based OSCs (SM/OM-OSCs), respectively [10e13]. However, only a few SMs exhibited a comparable photovoltaic performance in contrast to polymeric photovoltaic materials. The development of new photovoltaic SMs is still needed for high-performance SM-OSCs [13e16].

Generally, spectral response, absorption intensity, molecular orbital energy levels, charge mobility and film morphology have an important influence on photovoltaic performance of donor materials, which are mostly dominated by molecular structure [16e21]. To optimize these properties, alkyls in side chains, and the bridge length, central building blocks, end groups in skeleton, as well as the linkage positions of functional groups were tuned in the photovoltaic SMs [6,22e28]. On the other hand, a class of A-p-D-p-A type SMs was constructed to realize the above goal, which contains a central electron-donating (D) unit, two terminal electron-accepting (A) units and two p-conjugated bridges. There are several advantages for this kind of SMs applied in SM-OSCs, such as (i) high mobility with planar structure and efficient p-p interactions, (ii) a low bandgap, which is beneficial for intramolecular charge transfer, (iii) good film quality due to a long conjugated backbone and dispersed alkyl chains similar to polymers [29e31]. As a result, these A-p-D-p-A type SMs exhibited a significantly

* Corresponding author. College of Chemistry, Xiangtan University, Key Lab of Environment-Friendly Chemistry and Application in Ministry of Education, Xiangtan 411105, PR China.
** Corresponding author.
*** Corresponding author.
E-mail addresses: yangrq@qibebt.ac.cn (R. Yang), zhuwg18@126.com (W. Zhu).

http://dx.doi.org/10.1016/j.dyepig.2016.12.015
0143-7208/

increasing PCE of 10.08% in SM-OSCs [13].

In recent years, rhodanine was reported as a promising type of acceptor terminal unit in photovoltaic SMs owing to its strong electron-withdrawing property and effectively inducing intramolecular charge transfer [31e35]. By modifying rhodanine, tuning the D and p-bridge blocks, the A-p-D-p-A type SMs have showed a high PCE of 9%e10% [13,36]. While the arylene (Ar) hydrocarbon replaces those conjugated electron-rich D unit with heteroatom, it was further found that the A-p-Ar-p-A type SMs with a weak electron-donating Ar unit (phenylene or naphthylene) exhibited a deeper HOMO energy level than those analogues with stronger electron-donating D units (thiophene or thieno-thiophene), which presented higher V_{oc} value [37,38]. Our group recently obtained a similar type SM of $DPP_2An(2,6)$, which exhibited an increasing PCE of 5.44% and higher hole mobility of 4.02×10^{-4} cm^{-2} v^{-1} s^{-1} than DPP_2Ph and DPP_2Nap [39]. It indicates that the terminal A and central Ar units play an important role in improving photovoltaic properties for their resulting SMs.

In order to efficiently tune photovoltaic performance and further reveal influence of the central Ar and terminal A units on properties, a series of linear A-Ar-A type SMs of $(DRCN3T)_2Ar$ was primarily designed and synthesized. An Ar unit and 2-(1,1-dicyanomethylene) rhodanine (DRCN) were respectively used as central core and terminal acceptor, 5-vinyl-trithiophene (3T) was employed as space and insetted between Ar and A units in these SMs. The optophysical, electrochemical and photovoltaic properties were systematically investigated. Significant effect of the central Ar unit on these opto-electronic properties was observed in these SMs of $(DRCN3T)_2Ar$. The photovoltaic properties were remarkably improved in these SMs/$PC_{71}BM$-based solution-processing OSCs by enlarging Ar units in $(DRCN3T)_2Ar$. The best photovoltaic properties with a PCE of 5.15% and a short-circuit current density of 11.34 mA cm^{-2} were obtained in the $(DRCN3T)_2Ant$ based OSCs.

2. Experimental section

2.1. Materials

All starting materials, unless otherwise indicated, were purchased from commercial suppliers and used without further purification. Compounds 1, 2, 3, 4 and 5 were prepared according to the reported methods [40e42]. Three new photovoltaic SMs of $(DRCN3T)_2Ar$ were characterized by MS, ^1H NMR, and elemental analysis, which are consistent with their molecular structures.

2.2. Synthesis

2.2.1. Synthesis of $Ph(3TCHO)_2$

A solution of 1,4-benzenediboronic acid bis(pinacol) ester (78 mg, 0.235 mmol) and 5″-bromo-3,3″-dioctyl-[2,2′:5′,2″-terthiophene]-5-carbaldehyde (300 mg, 0.517 mmol) in toluene (8 mL) and 1 M aqueous sodium carbonate (Na_2CO_3) solution (2 mL) was degassed twice with argon. Then tetrakis(triphenylphosphine)palladium ($Pd(PPh_3)_4$, 10 mg, 0.026 mmol) and Aliquat 336 (0.05 mL) were added and the resulting mixture was stirred at 80 °C for 24 h under argon atmosphere. Cooled down to room temperature, the mixture was poured into water (60 mL), and extracted with chloroform ($CHCl_3$, 3 × 10 mL). The organic layer was dried over anhydrous sodium sulphate (Na_2SO_4). The solvent was removed off by a rotating evaporator and the residue was purified by silica gel chromatography using a mixture of petroleum ether (PE) and dichloromethane (DCM) (2:1) as eluent to provide red solid (151 mg, 60.0%). ^1H NMR (400 MHz, $CDCl_3$): δ 9.84 (s, 2H), 7.61 (s, 4H), 7.26 (s, 4H), 7.22 (s, 2H), 7.16 (d, J ¼4Hz, 2H), 2.87e2.76 (q, 8H), 1.74e1.66 (m, 8H), 1.47e1.40 (m, 8H), 1.34e1.26 (m, 32H), 0.90e0.86 (m, 12H). MS (MALDI-TOF) *m/z*: calcd for $C_{64}H_{82}O_2S_6$ $[M]^þ$, 1710.68; found, 1710.66.

2.2.2. Synthesis of $Nap(3TCHO)_2$

$Nap(3TCHO)_2$ was prepared according to the synthetic procedure of $Ph(3TCHO)_2$. A red solid of 200 mg was obtained with a yield of 68.0%. ^1H NMR (400 MHz, $CDCl_3$): δ 9.84 (s, 2H), 8.01 (s, 2H), 7.85 (d, J ¼ 8 Hz, 2H), 7.75 (d, J ¼ 8 Hz, 2H), 7.61 (s, 2H), 7.32 (s, 2H), 7.28 (s, 2H), 7.18 (d, J ¼ 4 Hz, 2H), 2.85e2.83 (q, 8H), 1.75e1.68 (m, 8H), 1.45e1.38 (m, 8H), 1.35e1.25 (m, 32H), 0.90e0.88 (m, 12H). MS (MALDI-TOF) *m/z*: calcd for $C_{68}H_{84}O_2S_6$ $[M]^þ$, 1124.48; found, 1124.679.

2.2.3. Synthesis of $Ant(3TCHO)_2$

$Ant(3TCHO)_2$ was prepared according to the synthetic procedure of $Ph(3TCHO)_2$. A red solid of 200 mg was obtained with yield of 70.0%. ^1H NMR (400 MHz, $CDCl_3$): δ 9.84 (s, 2H), 8.38 (s, 2H), 8.17 (s, 2H), 8.00 (d, J ¼ 8 Hz, 2H), 7.74 (d, J¼ 8 Hz, 2H), 7.61 (s, 2H), 7.36 (s, 2H), 7.28 (d, J¼ 4 Hz, 2H), 7.19 (d, J¼4 Hz, 1H), 2.86e2.84 (q, 8H), 1.76e1.70 (m, 8H), 1.48e1.42 (m, 8H), 1.35e1.25 (m, 32H), 0.89e0.87 (m, 12H). MS (MALDI-TOF) *m/z*: calcd for $C_{72}H_{86}O_2S_6$ $[M]^þ$, 1174.5; found, 1174.884.

2.2.4. Synthesis of $(DRCN3T)_2Ph$

$(3TCHO)_2Ph$ (177 mg, 0.165 mmol) and 2-(1,1-dicyanomethylene) rhodanine (318 mg, 1.65 mmol) was dissolved in a solution of dry chloroform (20 mL), then five drops of triethylamine were added. The mixture was stirred overnight under argon atmosphere at room temperature. The solvent was then removed off with a rotating evaporator. The residue was dissolved in 8 mL of chloroform and precipitated from methanol. The precipitate was filtered off and purified by silica gel chromatography using a mixture of PE and chloroform (1:1) as eluent to produce black solid (180 mg, 77.0%). ^1H NMR (400 MHz, $CDCl_3$): δ 8.00 (s, 2H), 7.61 (s, 4H), 7.32 (s, 2H), 7.31 (s, 2H), 7.22 (s, 2H), 7.18 (d, J ¼ 4 Hz, 2H), 4.35e4.30 (q, 4H), 2.88e2.81 (q, 8H), 1.73e1.69 (m, 8H), 1.44e1.42 (m, 14H), 1.33e1.25 (s, 32H), 0.91e0.88 (s, 12H). MS (MALDI-TOF) *m/z*: calcd for $C_{80}H_{92}N_6O_2S_8$, $[M]^þ$, 1424.50; found, 1424.658. Elemental analysis for $C_{80}H_{92}N_6O_2S_8$: calcd. C, 67.37; H, 6.50; N, 5.89; S, 17.99; found C, 67.10; H, 6.32; N, 5.73; S, 18.12.

2.2.5. Synthesis of $(DRCN3T)_2Nap$

$(DRCN3T)_2Nap$ was prepared according to the synthetic procedure of $(DRCN3T)_2Ph$. A black solid of 120 mg was obtained with a yield of 80.0%. ^1H NMR (400 MHz, $CDCl_3$): δ 8.01 (d, J¼ 8 Hz, 4H), 7.86 (d, J ¼8 Hz, 2H), 7.76 (d, J ¼8 Hz, 2H), 7.33 (s, 4H), 7.31 (s, 2H), 7.20 (d, J ¼4 Hz, 2H), 4.35e4.30 (q, 4H), 2.89e2.84(q, 8H), 1.80e1.70 (m, 8H), 1.46e1.40 (m, 14H), 1.34e1.25 (m, 32H), 0.92e0.88 (m, 12H). MS (MALDI-TOF) *m/z*: calcd for $C_{84}H_{94}N_6O_2S_8$ $[M]^þ$, 1474.52; found, 1474.890. Elemental analysis for $C_{84}H_{94}N_6O_2S_8$: calcd. C, 68.34; H, 6.42; N, 5.69; S, 17.38; found C, 68.10; H, 6.35; N, 5.73; S, 17.15.

2.2.6. Synthesis of $(DRCN3T)_2Ant$

$(DRCN3T)_2Ant$ was prepared according to the synthetic procedure of $(DRCN3T)_2Ph$. A black solid of 180 mg was obtained with a yield of 82.0%. ^1H NMR (400 MHz, $CDCl_3$): δ 8.34 (s, 2H), 8.14 (s, 2H), 7.98 (d, J ¼ 12 Hz,4H), 7.72 (d, J¼8 Hz, 2H), 7.35 (s, 2H), 7.31 (d, J ¼2 Hz, 2H), 7.28 (s, 2H), 7.20 (d, J¼ 2 Hz, 2H), 4.31e4.27 (q, 4H), 2.88e2.83 (q, 8H), 1.78e1.69 (m, 8H), 1.45e1.35 (m, 14H), 1.35e1.25 (m, 32H), 0.91e0.87 (m, 12H). MS (MALDI-TOF) *m/z*: calcd for $C_{88}H_{96}N_6O_2S_8$ $[M]^þ$, 1524.54; found, 1524.834. Elemental analysis for $C_{88}H_{96}N_6O_2S_8$: calcd. C, 69.25; H, 6.34; N, 5.51; S, 16.81; found C, 69.08; H, 6.12; N, 5.23; S, 16.40.

2.3. Measurements and characterization

All ^{1}H NMR spectra were recorded on a Bruker DRX-400 spectrometer using $CDCl_3$ as solvent at 298 K. Mass spectra were made on a Bruker Daltonics BIFLEX III MALDI-TOF analyzer. Thermogravimetric analyses (TGA) were conducted under a dry nitrogen gas flow at a heating rate of 10 ^{0}C min^{-1} on a PerkineElmer TGA 7. The differential scanning calorimetry (DSC) was measured on a TA DSCQ-10 instrument at a heating/cooling rate of 10 ^{0}C min^{-1} under a nitrogen atmosphere. UVeVis absorption spectra were recorded on a HP-8453 UV visible system. Cyclic voltammetry (CV) was carried out on a CHI660A electrochemical work-station in a three-electrode cell at room temperature, which was dipped in a 0.1 M tetrabutyl-ammonium hexa-fluorophosphate (Bu_4NPF_6) acetonitrile solution under nitrogen protection at a scan rate of 100 mV/s. In this three-electrode cell, a platinum rod, platinum wire and Ag/AgCl (0.1 M) electrode were used as a working electrode, counter electrode and reference electrode, respectively. The morphology of active layers was examined by transmission electron microscope (TEM), which was carried out on a FEI Tecnai T20 with LaB6 operated at 200 kV. The active layer used as TEM measurement was placed onto a copper grid after dissolving the PEDOT: PSS in water [43,44].

2.4. Device fabrication and characterization

OSCs were fabricated using indium tin oxide (ITO) glass as an anode, Ca/Al as a cathode, and a blend film of the SM/$PC_{71}BM$ as a photosensitive layer, respectively. After a 30 nm buffer layer of poly(3,4-ethylenedioxy-thiophene) and polystyrene sulfonic acid (PEDOT:PSS) was spin-coated onto the precleaned ITO substrate, the photosensitive layer was subsequently prepared by spin-coating a solution of the SM/$PC_{71}BM$ (1:3, w/w) in $CHCl_3$ on the PEDOT:PSS layer with a typical concentration of 10 mg mL^{-1}. The resulting substrates were dried under nitrogen at room temperature in a nitrogen-filled glove-box. Ca (10 nm) and Al (100 nm) were successively deposited on the photosensitive layer in vacuum and used as top electrodes. The current density-voltage (*J-V*) characteristics of the devices were carried out on a computer controlled Keithley 236 source measurement system under simulated 100 mW cm^{-2} (AM 1.5 G) irradiation from a Newport solar simulator. Light intensity was calibrated with a standard silicon solar cell. The active area was 0.1 cm^{-2} each cell. The thicknesses of the spun-cast films were recorded by a profilometer (Alpha-Step 200, Tencor Instruments). The external quantum efficiency (*EQE*) was measured with a Stanford research systems model SR830 DSP lock-in amplifier coupled with WDG3 monochromator and a 150 W xenon lamp.

3. Results and discussion

3.1. Synthesis, thermal property and crystallinity

The general synthetic routes for these SMs of $(DRCN3T)_2Ph$, $(DRCN3T)_2Nap$ and $(DRCN3T)_2Ant$ are outlined in Scheme 1. They were obtained with a yield about 80%. Their molecular structures are confirmed by the ^{1}H NMR and MALDI-MS measurement, which are consistent with molecular formulas.

The thermal stability of these SMs was investigated by TGA under the nitrogen atmosphere. The corresponding TGA curves and

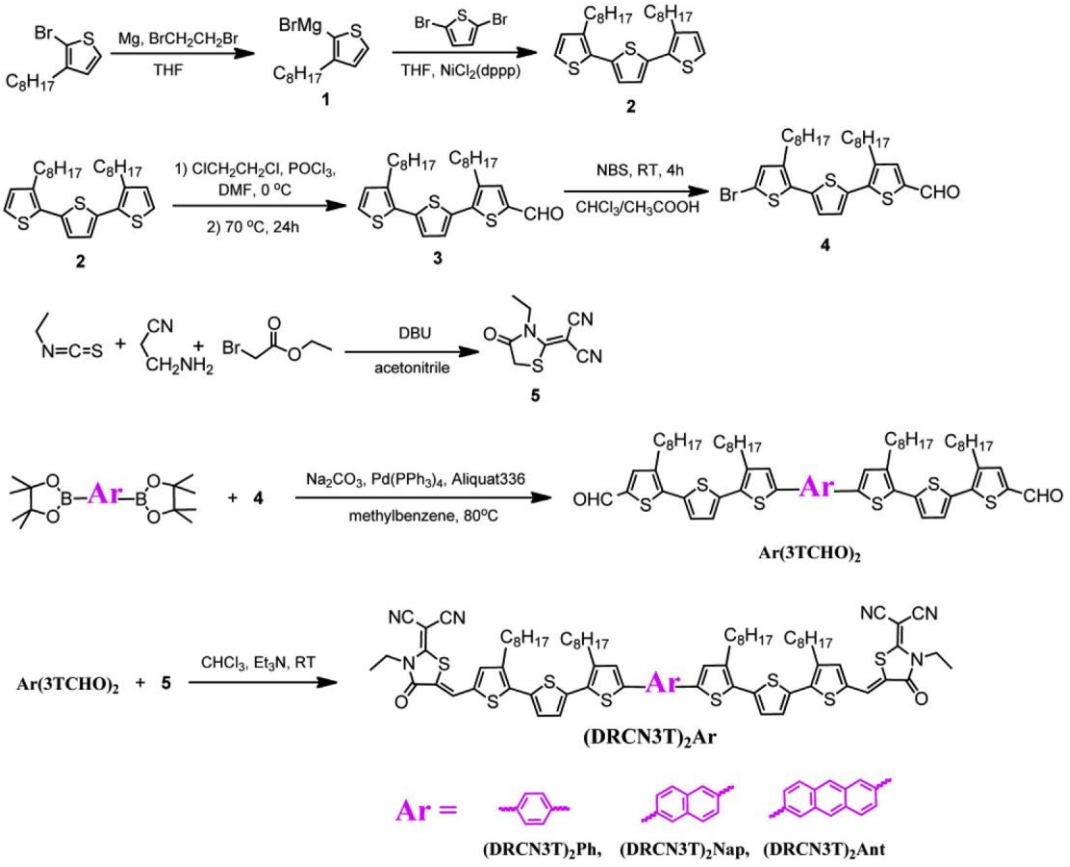

Scheme 1. Synthetic routes of $(DRCN3T)_2Ph$, $(DRCN3T)_2Nap$ and $(DRCN3T)_2Ant$.

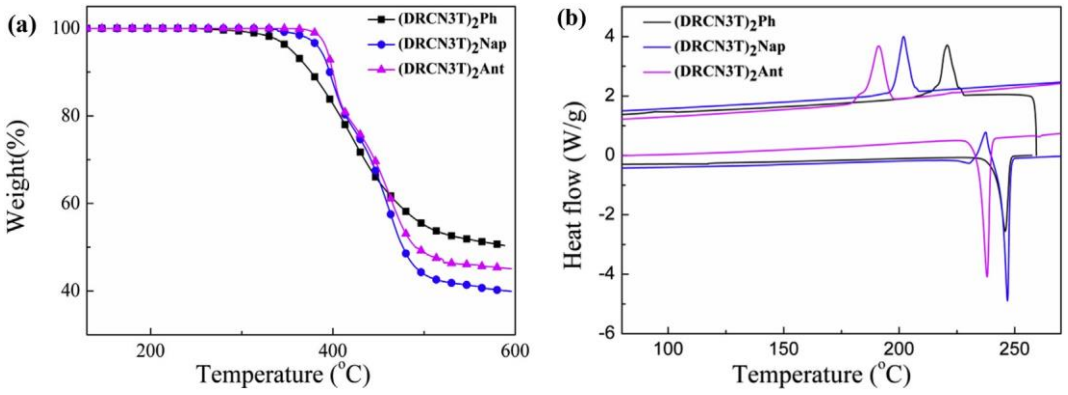

Fig. 1. (a) TGA curves at a heating rate of 10 ^{0}C min^{-1} under nitrogen atmosphere and (b) DSC curves at a heating/cooling rate of 10 ^{0}C min^{-1} under nitrogen atmosphere for $(DRCN3T)_2Ph$, $(DRCN3T)_2Nap$ and $(DRCN3T)_2Ant$.

Table 1
Optical and electrochemical data of $(DRCN3T)_2Ph$, $(DRCN3T)_2Nap$ and $(DRCN3T)_2Ant$.

Molecules	$\varepsilon(\lambda_{max})$ (M^{-1} cm^{-1})	λ_{max} (nm)[a]	λ_{max} (nm)[b]	λ_{onset} (nm)[c]	E_g^{opt} (eV)	E_{HOMO} (eV)	E_{LOMO} (eV)	E_g^{elec} (eV)	T_d (^{0}C)
$(DRCN3T)_2Ph$	7.8×10^4	521	579	706	1.76	—5.27	—3.57	1.70	354
$(DRCN3T)_2Nap$	7.6×10^4	520	601	741	1.67	—5.25	—3.56	1.69	387
$(DRCN3T)_2Ant$	6.2×10^4	523	585,625	763	1.63	—5.22	—3.57	1.65	394

[a] Measured in $CHCl_3$.
[b] Measured in the thin film.
[c] E_g^{opt} ¼ 1240/λ_{onset}.

data were depicted in Fig. 1 (a) and Table 1, respectively. The thermal decomposition temperatures (T_d) of 354, 387, 394 ^{0}C are exhibited for $(DRCN3T)_2Ph$, $(DRCN3T)_2Nap$, $(DRCN3T)_2Ant$ at 5% weight loss, respectively. It implies that all of three SMs here have good thermal stability. Further-more, the $(DRCN3T)_2Ant$ with bigger Ar rings shows better thermal stability than $(DRCN3T)_2Ph$ and $(DRCN3T)_2Nap$. Therefore, properly extending the central Ar ring could enhance thermal stability, which is similar to the phenomena reported in our previous work. Fig. 1 (b) depicts the differential scanning calorimetry (DSC) plots of SMs in solid state. The typical endothermal peaks at 245, 247 and 237 ^{0}C are observed for $(DRCN3T)_2Ph$, $(DRCN3T)_2Nap$, $(DRCN3T)_2Ant$ during heating process, which correspond to melting temperatures (T_m), respectively. Moreover, $(DRCN3T)_2Ph$, $(DRCN3T)_2Nap$ and $(DRCN3T)_2Ant$ also display an exothermal peak at 220, 201, 190 ^{0}C during cooling process, respectively. It indicates that three SMs possess good crystallinity.

3.2. Optical properties

The normalized UVeVis absorption spectra of $(DRCN3T)_2Ph$, $(DRCN3T)_2Nap$ and $(DRCN3T)_2Ant$ in dilute $CHCl_3$ solution and in their pure/blend films are shown in Fig. 2 (a). Their corresponding absorption data are summarized in Table 1. Strong and broad absorption bands in the visible to near-infrared region are observed for these three SMs. In the solution states, all of three SMs exhibit the same absorption peak at ~521 nm in the low-lying region, that are independent of the central Ar units. The similar absorption may be contributed to the similar conjugation length of these series of molecules mainly governed by the six thiophenes units together with the two conjugated end units [13]. In the solid states, all of them display a broader and obvious red-shifted absorption peak by 50e100 nm in the low-lying region in comparison to those in their solution absorption profiles. It indicates that ordered structure and strong p-p stacking effect, as well as intermolecular interaction should exist between the molecular backbones in the solid pure films. It is noteworthy that the $(DRCN3T)_2Ant$ films shows a larger red-shifted by 103 nm and a distinct shoulder at 625 nm, which result from a more effective molecular packing between molecular backbones by the effect of a lager conjugated anthracene. Based on the onset of the pure film absorption, the optical band gaps (E_g^{opt}) of $(DRCN3T)_2Ph$, $(DRCN3T)_2Nap$, $(DRCN3T)_2Ant$ are calculated to be 1.76, 1.67 and 1.63 eV, respectively.

Compared to the pure films, it is found that the SM/$PC_{71}BM$ blend films shows an increasing absorption in the range of 400e500 nm, as showed in Fig. 2 (b), which is assigned to the contribution of $PC_{71}BM$. While those blend films are processed by 1,8-diiodooctane (DIO) additive, the $(DRCN3T)_2Ant$ blend film further demonstrates a little increasing absorption intensity. In contrast, the $(DRCN3T)_2Ph$ and $(DRCN3T)_2Nap$ blend films display a little decreasing absorption intensity. It indicates that adding the DIO solvent additive in the $(DRCN3T)_2Ant$ blend films is in favour of improving intermolecular interaction.

3.3. Electrochemical properties

The electrochemical properties were characterized by cyclic voltammetry (CV) method, in which oxidation and reduction potentials were calibrated using the ferrocene/ferrocenium ($Fc/Fc^þ$) redox couple (4.8 eV below the vacuum level). The energy levels of the highest occupied molecular orbital (HOMO) and lowest unoccupied molecular orbital (LUMO) are calculated from the onset oxidation and reduction potentials, respectively. The recorded CV curves are shown in Fig. 3 and the relevant data are summarized in Table 1. It is found that the HOMO energy levels (E_{HOMO}) have a little increase from —5.27, —5.25 to —5.22 eV with the increasing Ar rings from Ph, Nap to Ant in $(DRCN3T)_2Ar$. But their LUMO energy levels (E_{LUMO}) are almost similar values at –3.56 ~ –3.57 eV, which are largely dominated by the same electron-deficient ending groups. The resulting electrochemical band gaps of $(DRCN3T)_2Ph$, $(DRCN3T)_2Nap$ and $(DRCN3T)_2Ant$ are estimated to be 1.70, 1.69, 1.65 eV respectively, which are consistent with their optical band gaps.

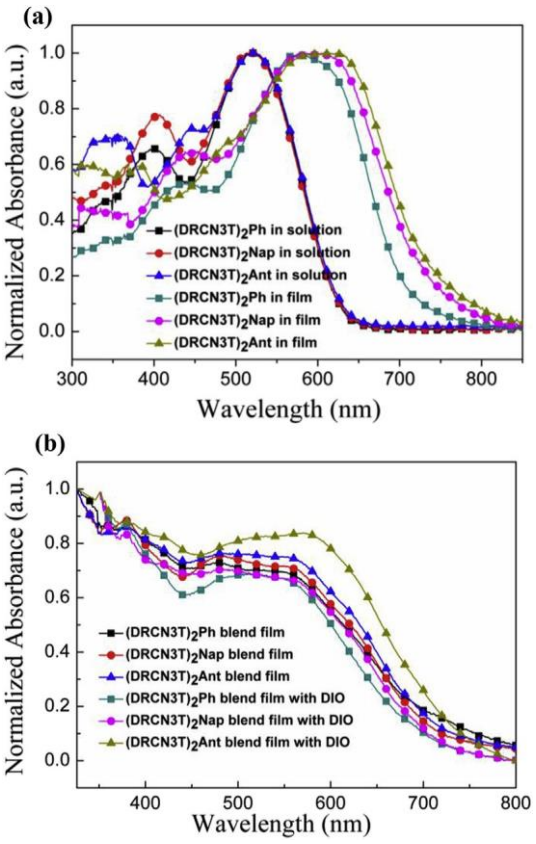

Fig. 2. UVevis absorption spectra of $(DRCN3T)_2Ph$, $(DRCN3T)_2Nap$ and $(DRCN3T)_2Ant$ in $CHCl_3$ solutions and in pure films (a), blend films without DIO additive and blend films with 2% DIO additive (b).

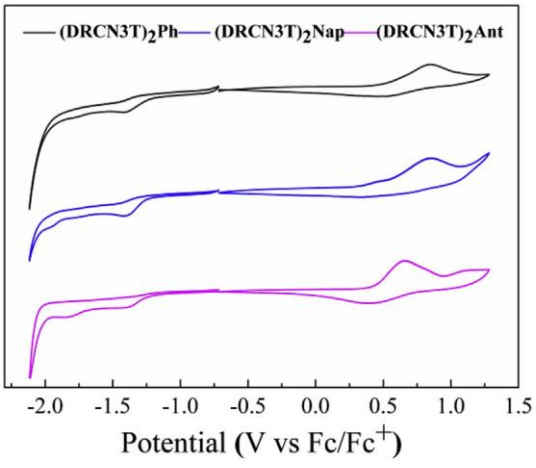

Fig. 3. Cyclic voltammetry curves of $(DRCN3T)_2Ph$, $(DRCN3T)_2Nap$ and $(DRCN3T)_2Ant$.

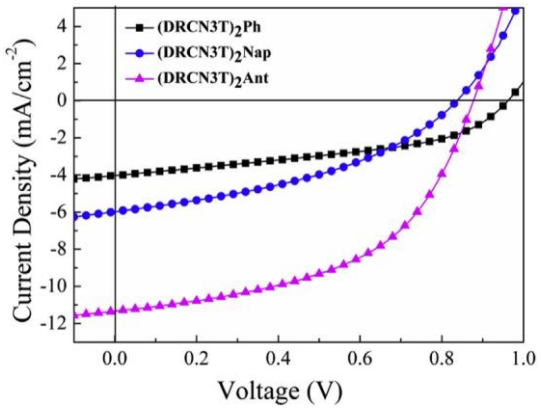

Fig. 4. *J-V* curves of three SM-based OSCs at optimized processing conditions under the illumination of AM 1.5 G, 100 mW cm^{-2}.

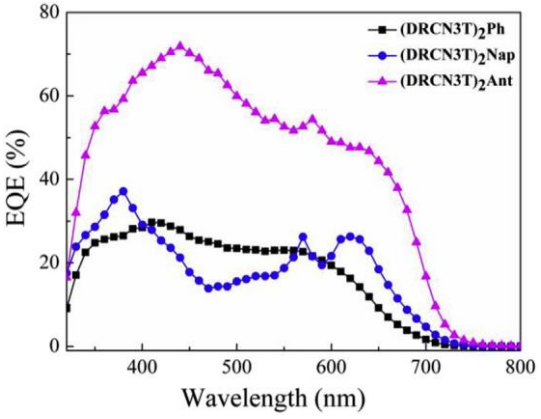

Fig. 5. *EQE* curves of the $(DRCN3T)_2Ph$, $(DRCN3T)_2Nap$ and $(DRCN3T)_2Ant$ based devices at the optimized processing conditions.

3.4. Photovoltaic properties

The photovoltaic properties of these linear SMs were investigated in their bulk heterojunction OSCs with a structure of ITO/PEDOT:PSS/SM:$PC_{71}BM$/Ca/Al. The device fabrication processes are described in detail in the experimental section. The ratios between SM and $PC_{71}BM$ were changed from 1:2, 1:3 to 1:4, as well as the doping concentrations of the DIO additive were tuned from 0%, 1%, 2%e3% in order to optimize processing technology. The measured photovoltaic data of the SM/$PC_{71}BM$ based cells are listed in Table S1 and S2. It demonstrates that the optimized SM/$PC_{71}BM$ ratio is the same at 1:3, but the DIO additive has played different rule in different devices. For the $(DRCN3T)_2Ph$ and $(DRCN3T)_2Nap$ based cells, adding DIO additive destroys device performance. In contrast, adding 2% DIO additive makes the $(DRCN3T)_2Ant$ based cell exhibit the best device performance. The optimized photovoltaic performances for the $(DRCN3T)_2Ph$, $(DRCN3T)_2Nap$ and $(DRCN3T)_2Ant$

Table 2
Photovoltaic performance of the SM/$PC_{71}BM$ OSCs and the hole mobilities of the SM/$PC_{71}BM$ blend films.

SM	D:A (w/w)	V_{oc} (V)	J_{sc} (mA/cm^2)	*FF* (%)	PCE (%)	m_h ($cm^2v^{-1}s^{-1}$)	m_e ($cm^2v^{-1}s^{-1}$)
$(DRCN3T)_2Ph$	1:3	0.97 ± 0.01	4.03 ± 0.11	43 ± 1	1.64 ± 0.05 (1.74)	6.56×10^{-6}	2.80×10^{-4}
$(DRCN3T)_2Nap$	1:3	0.98 ± 0.01	4.15 ± 0.18	48 ± 2	1.97 ± 0.03 (2.01)	1.44×10^{-4}	2.52×10^{-4}
$(DRCN3T)_2Ant$	1:3	0.95 ± 0.01	4.50 ± 0.11	51 ± 1	2.18 ± 0.06 (2.29)	e	e
$(DRCN3T)_2Ant$[a]	1:3	0.87 ± 0.01	11.08 ± 0.30	53 ± 2	5.11 ± 0.02 (5.15)	2.74×10^{-4}	2.86×10^{-4}

[a] 2% DIO additive. The average PCEs was obtained from over 5 devices. The best PCEs are provided in parentheses.

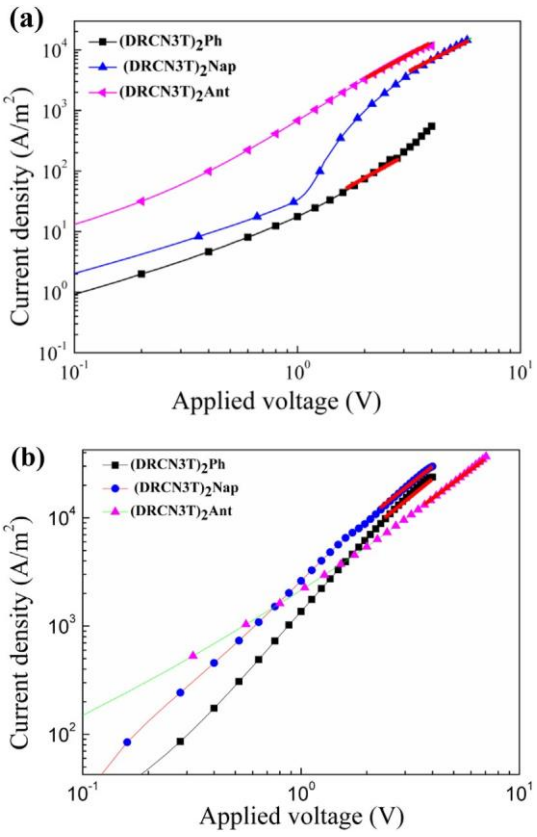

Fig. 6. *J-V* characteristics of the optimized hole-only (a) and electron-only (b) devices based on $(DRCN3T)_2Ph$, $(DRCN3T)_2Nap$ and $(DRCN3T)_2Ant$.

based cells are listed in Table 2. The corresponding current density *vs* voltage (*J-V*) curves are shown in Fig. 4 measured under AM 1.5G irradiation at an intensity of 100 mW cm^{-2}. Under the optimized conditions, the PCE and short-circuit current density (J_{sc}) values are obviously improved from the $(DRCN3T)_2Ph$ and $(DRCN3T)_2Nap$ based cells to the $(DRCN3T)_2Ant$ based cell, whereas open-circuit voltage (V_{oc}) values have a little decrease. The best photovoltaic performances with a PCE of 5.15% and J_{sc} of 11.38 mA cm^{-2} were obtained in the $(DRCN3T)_2Ant$ based cell at the optimized processing conditions. The results here further indicate that properly extending the central Ar ring could be beneficial to improve photovoltaic properties for the A-Ar-A type SMs [33e35].

To further understand why the $(DRCN3T)_2Ant$ based cell exhibited the highest J_{sc} value among these cells, the external quantum efficiency (*EQE*) curves of these devices under the optimized processing conditions were measured and shown in Fig. 5. A broad photo-response region with different *EQE* values in the region of 330e700 nm is analogously observed for these devices. The $(DRCN3T)_2Ant$ based device displays a significantly improved *EQE* of 73% in comparison to the $(DRCN3T)_2Ph$ and the $(DRCN3T)_2Nap$ based cells. It indicates that introducing central Ant ring is available to increase *EQE* value for its SM, which is available to promote the increase of the J_{sc} value.

In order to explain why the $(DRCN3T)_2Ant$ based cell exhibited the highest *FF* value, the hole and electron mobilities of three SMs were measured in their hole and electron-only devices using the space charge limited current (SCLC) method, respectively. The *J-V* characteristics in the dark are depicted in Fig. 6 (a) and (b) for these optimized hole- and electron-only devices, respectively. An increasing hole mobility is observed from 6.56×10^{-6} to 1.44×10^{-4} and 2.74×10^{-4} $cm^2v^{-1}s^{-1}$ in the hole-only $(DRCN3T)_2Ph$, $(DRCN3T)_2Nap$ and $(DRCN3T)_2Ant$ based devices, respectively. However, the electron mobilities of three SMs have a little change in a range of $2.52 \times 10^{-4} \sim 2.86 \times 10^{-4}$ $cm^2v^{-1}s^{-1}$. It is clear that $(DRCN3T)_2Ant$ presents much higher hole mobility and more balanced carrier mobility than $(DRCN3T)_2Ph$ and $(DRCN3T)_2Nap$, which is consistent with the corresponding *FF* and J_{sc} results. It firmly demonstrates that properly extending the central Ar ring can increase hole mobility and balance carrier mobility due to better molecular packing of the enlarged Ar ring.

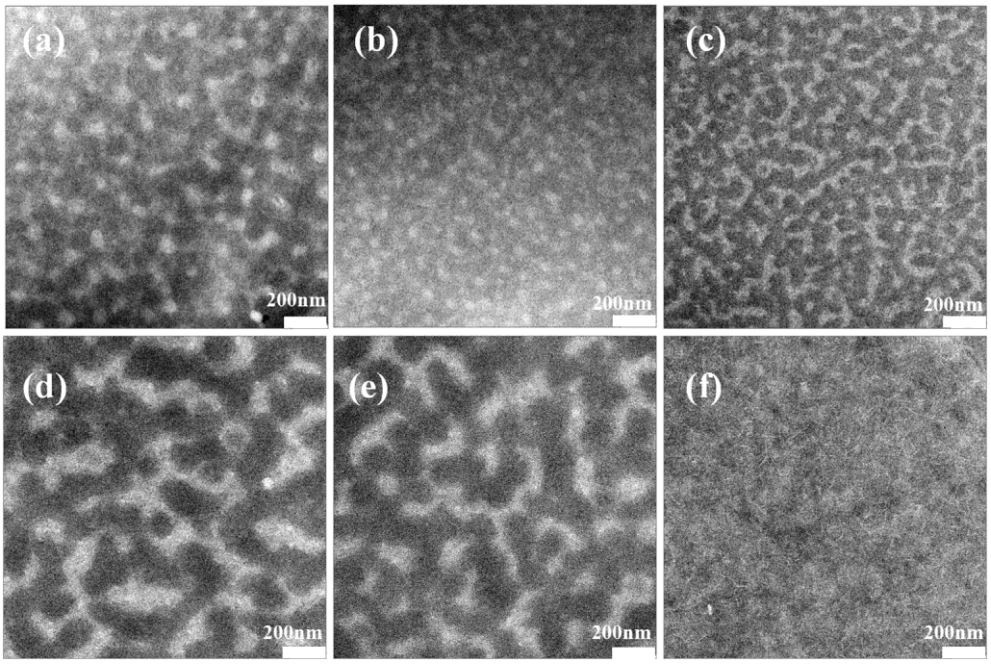

Fig. 7. TEM images of the SM:$PC_{71}BM$ (1:3, w/w) blend films for $(DRCN3T)_2Ph$ (a,d), $(DRCN3T)_2Nap$ (b,e) and $(DRCN3T)_2Ant$ (c,f) without/with 2%DIO additive.

The morphologies of the SM/$PC_{71}BM$ blend films under the optimized processing conditions were recorded with transmission electron microscopy (TEM) and shown in Fig. 7. The observed dark phases are assigned to the $PC_{71}BM$ domains because of its relatively higher electron scattering density [39,45]. The fibrillar structure with a width around 30e60 nm are exhibited in these TEM images for the SM/$PC_{71}BM$ blend films without DIO additive (Fig. 7a, b and c). While the 2% DIO additive is added, the $(DRCN3T)_2Ant$ blend film show a continuous acicular fibrous structure with a decreased size of 14 nm (Fig. 7f). It means that a continuously interpenetrated network is formed in the $(DRCN3T)_2Ant$ blend film processed by DIO additive, which is favorable for the charge transportation. However, the $(DRCN3T)_2Ph$ and $(DRCN3T)_2Nap$ blend films show a significantly dispersed phase structures after processed by 2% DIO additive (Fig. 7d and e). It implies that the DIO additive has promotes molecular self-aggregation for $(DRCN3T)_2Ph$ and $(DRCN3T)_2Nap$ blend films. It further explains why the $(DRCN3T)_2Ant$ based cells exhibited higher *FF* values than the $(DRCN3T)_2Ph$ and $(DRCN3T)_2Nap$ based cells.

4. Conclusions

Three linear A-Ar-A type SMs of $(DRCN3T)_2Ph$, $(DRCN3T)_2Nap$ and $(DRCN3T)_2Ant$ were obtained. The influence of the central Ar unit on optical, electrochemical and photovoltaic properties was presented. With enlarging the central Ar ring from phenylene, naphthalene to anthracene, the A-Ar-A type SMs of $(DRCN3T)_2Ar$ exhibited the much improved PCE and J_{sc} values. The best photovoltaic performance with a PCE of 5.15% was obtained in the $(DRCN3T)_2Ant/PC_{71}BM$ based cell, which is three times of that in the $(DRCN3T)_2Ph/PC_{71}BM$ based device.

Acknowledgements

Thanks to the financial supports from the Major Cultivation and General Programs of the National Natural Science Foundation of China (51673031, 91233112, 21172187, 51403178), the Program for Innovative Research Cultivation Team in University of Ministry of Education of China (1337304), the Natural Science Foundation of Hunan (14JJ4019, 2015JJ3113), Open Project for the National Key Laboratory of Luminescent Materials and Devices (2014-skllmd-10), the Hunan Postgraduate Science Foundation for Innovation (CX2014B257, CX2015B201).

Appendix A. Supplementary data

Supplementary data related to this article can be found at http://dx.doi.org/10.1016/j.dyepig.2016.12.015.

References

[1] Cheng YJ, Yang SH, Hsu CS. Synthesis of conjugated polymers for organic solar cell applications. Chem Rev 2009;109:5868e923.
[2] Li ZF, Dong QF, Li YW, Xu B, Deng M, Pei JN, et al. Design and synthesis of solution processable small molecules towards high photovoltaic performance. J Mater Chem 2011;21:2159e68.
[3] Chen YS, Wan XJ, Long GK. High performance photovoltaic applications using solution-processed small molecules. Acc Chem Res 2013;46:2645e55.
[4] Coughlin JE, Henson ZB, Welch GC, Bazan GC. Design and synthesis of molecular donors for solution-processed high-efficiency organic solar cells. Acc Chem Res 2014;47:257e70.
[5] Walker B, Kim C, Nguyen TQ. Small molecule solution-processed bulk heterojunction solar cells. Chem Mater 2010;23:470e82.
[6] Zhou P, Dang DF, Wang Q, Duan XW, Xiao MJ, Tao Q, et al. Enhancing the photovoltaic performance of triphenylamine based star-shaped molecules by tuning the moiety sequence of their arms in organic solar cells. J Mater Chem A 2015;3:13568e76.
[7] Wang JL, Yin QR, Miao JS, Wu Z, Chang ZF, Cao Y, et al. Rational design of small molecular donor for solution processed organic photovoltaics with 8.1% efficiency and high fill factor via multiple fluorine substituents and thiophene bridge. Adv Funct Mater 2015;25:3514e23.
[8] Wang JL, Xiao F, Yan J, Wu Z, Liu KK, Chang ZF, et al. Difluorobenzothiadiazole-based small-molecule organic solar cells with 8.7% efficiency by tuning of p-conjugated spacers and solvent vapor annealing. Adv Funct Mater 2016;26:1803e12.
[9] Wang JL, Liu KK, Yan J, Wu Z, Liu F, Xiao F, et al. Series of multifluorine substituted oligomers for organic solar cells with efficiency over 9% and fill factor of 0.77 by combination thermal and solvent vapor annealing. J Am Chem Soc 2016;138:7687e97.
[10] You JB, Dou LT, Yoshimura K, Kato T, Ohya K, Moriarty T, et al. A polymer tandem solar cell with 10.6% power conversion efficiency. Nat Commun 2013;4:66e78.
[11] Liu YH, Zhao JB, Li ZK, Mu C, Ma W, Hu HW, et al. Aggregation and morphology control enables multiple cases of high-efficiency polymer solar cells. Nat Commun 2014;5. 5293e5293.
[12] Liu C, Yi C, Wang K, Yang YL, Bhatta R, Tsige M, et al. Single junction polymer solar cells with over 10% efficiency by novel two-dimensional donor-acceptor conjugated copolymer. ACS Appl Mater Interfaces 2015;7:4928e35.
[13] Kan B, Li MM, Zhang Q, Liu F, Wan XJ, Wang YC, et al. A series of simple oligomer-like small molecules based on oligothiophenes for solution-processed solar cells with high efficiency. J Am Chem Soc 2015;137:3886e93.
[14] Gao K, Li LS, Lai TQ, Xiao LG, Huang Y, Huang F, et al. Deep absorbing porphyrin small molecule for high performance organic solar cells with very low energy losses. J Am Chem Soc 2015;137:7282e5.
[15] Mishra A, Bäuerle P. Small molecule organic semiconductors on the move: promises for future solar energy technology. Angew Chem Int Ed 2012;51:2020e67.
[16] Kan B, Zhang Q, Liu F, Wan XJ, Wang YC, Ni W, et al. Small molecules based on alkyl/Alkylthio-thieno [3,2-b] thiophene-substituted benzo [1,2-b:4,5-b'] dithiophene for solution-Processed solar cells with high performance. Chem Mater 2015;27:8414e23.
[17] Su WY, Fan QP, Xiao MJ, Chen JH, Zhou P, Liu B, et al. Improved photovoltaic performance of a side-chain D-A polymer in polymer solar cells by shortening the phenyl spacer between the D and A units. Macromol Chem Phys 2014;215:2075e83.
[18] Zhang MJ, Guo X, Ma W, Zhang SQ, Huo LJ, Ade H, et al. An easy and effective method to modulate molecular energy level of the polymer based on benzodithiophene for the application in polymer solar cells. Adv Mater 2014;26:2089e95.
[19] Zhang MJ, Guo X, Ma W, Ade H, Hou JH. A large-bandgap conjugated polymer for versatile photovoltaic applications with high performance. Adv Mater 2015;27:4655e60.
[20] Fan QP, Su WY, Guo X, Guo B, Li WB, Zhang YD, et al. A new polythiophene derivative for high efficiency polymer solar cells with PCE over 9%. Adv Energy Mater 2016;6:1600430.
[21] Zhang MJ, Guo X, Zhang SQ, Hou JH. Synergistic effect of fluorination on molecular energy level modulation in highly efficient photovoltaic polymers. Adv Mater 2014;26:1118e23.
[22] Li WW, Hendriks KH, Furlan A, Roelofs WSC, Meskers SCJ, Wienk MM, et al. Effect of the fibrillar microstructure on the efficiency of high molecular weight diketopyrrolopyrrole-based polymer solar cells. Adv Mater 2014;26:1565e70.
[23] Zhang MJ, Guo X, Ma W, Ade H, Hou JH. A polythiophene derivative with superior properties for practical application in polymer solar cells. Adv Mater 2014;26:5880e5.
[24] Yan WB, Zhang Q, Qin QS, Ye SY, Lin YW, Liu ZW, et al. Design, synthesis and photophysical properties of A-D-A-D-A small molecules for photovoltaic application. Dyes Pigm 2015;121:99e108.
[25] Bai HT, Wang YF, Cheng P, Li YF, Zhu DB, Zhan XW. Acceptor-donor-acceptor small molecules based on indacenodithiophene for efficient organic solar cells. ACS Appl Mater Interfaces 2014;6:8426e33.
[26] Liu YS, Zhou JY, Wan XJ, Chen YS. Synthesis and properties of acceptor-donor-acceptor molecules based on oligothiophenes with tunable and low band gap. Tetrahedron 2009;65:5209e15.
[27] He GR, Li Z, Wan XJ, Liu YS, Zhou JY, Long GK, et al. Impact of dye end groups on acceptor-donor-acceptor type molecules for solution-processed photovoltaic cells. J Mater Chem 2012;22:9173e80.
[28] Li S, He ZC, Yu J, Chen SA, Zhong AS, Tang RL, et al. How the linkage positions affect the performance of bulk-heterojunction polymer solar cells. J Mater Chem 2012;22:12523e31.
[29] Kumara CV, Cabau L, Koukaras EN, Sharmab GD, Palomares E. Synthesis, optical and electrochemical properties of the A-p-D-p-A porphyrin and its application as an electron donor in efficient solution processed bulk heterojunction solar cells. Nanoscale 2015;7:179e89.
[30] Kumar CV, Cabau L, Koukaras EN, Sharma A, Sharmab GD, Palomares E. A-p-D-p-A based porphyrin for solution processed small molecule bulk heterojunction solar cells. J Mater Chem 2015;3:16287e301.
[31] Kan B, Zhang Q, Li MM, Wan XJ, Ni W, Long GK, et al. Solution-processed organic solar cells based on dialkylthiol-substituted benzodithiophene unit with efficiency near 10%. J Am Chem Soc 2014;136:15529e32.
[32] Zhou JY, Yi Z, Wan XJ, Long GK, Zhang Q, Ni W, et al. Solution-processed and high-performance organic solar cells using small molecules with a benzodithiophene unit. J Am Chem Soc 2013;135:8484e7.
[33] Zhou JY, Wan XJ, Liu YS. Small molecules based on benzo[1,2-b:4,5-b'] dithiophene unit for high-performance solution-processed organic solar cells.

J Am Chem Soc 2012;134:16345e51.
[34] Lim N, Cho N, Paek S, Kim C, Lee JK, Ko J. High-performance organic solar cells with efficient semiconducting small molecules containing an electron-rich benzodithiophene derivative. Chem Mater 2014;26:2283e8.
[35] Ni W, Li MM, Liu F, Wan XJ, Feng HR, Kan B, et al. Dithienosilole-based small-molecule organic solar cells with an efficiency over 8%: investigation of the relationship between the molecular structure and photovoltaic performance. Chem Mater 2015;27:6077e84.
[36] Zhang Q, Kan B, Liu F, Long GK, Wan XJ, Chen XQ, et al. Small-molecule solar cells with efficiency over 9%. Nat Phot 2015;9:35e41.
[37] Lee JW, Choi YS, Jo WH. Diketopyrrolopyrrole-based small molecules with simple structure for high Voc organic photovoltaics. Org Electron 2012;13:3060e6.
[38] Choi YS, Jo WH. A strategy to enhance both Voc and Jsc of A-D-A type small molecules based on diketopyrrolopyrrole for high efficient organic solar cells. Org Electron 2013;14:1621e8.
[39] Duan XW, Xiao MJ, Chen JH, Wang XD, Peng WH, Duan LR, et al. Improving photovoltaic performance of the linear A-Ar-A-type small molecules with diketopyrro-pyrroles arms by tuning the linkage position of anthracene core. ACS Appl Mater Interfaces 2015;7:18292e9.
[40] Fan QP, Li M, Yang PG, Liu Y, Xiao MJ, Wang XD, et al. Acceptor-donor-acceptor small molecules containing benzo[1,2-b:4,5- b'] dithiophene and rhodanine units for solution processed organic solar cells. Dyes Pigm 2015;116:13e9.
[41] Zhou JY, Wan XJ, Liu YS, Long GK, Wang F, Li Z, et al. A planar small molecule with dithienosilole core for high efficiency solution-processed organic photovoltaic cells. Chem Mater 2011;23:4666e8.
[42] Higashijima S, Miura H, Fujita T, Kubota Y, Funabiki K, Yoshida T, et al. Highly efficient new indoline dye having strong electron-withdrawing group for zinc oxide dye-sensitized solar cell. Tetrahedron 2011;67:6289e93.
[43] Su WY, Fan QP, Guo X, Guo B, Li WB, Zhang YD, et al. Efficient ternary blend all-polymer solar cells with a polythiophene derivative as a hole-cascade material. J Mater Chem A 2016;4:14752e60.
[44] Wan Q, Guo X, Wang ZY, Li WB, Guo B, Ma W, et al. 10.8% Efficiency polymer solar cells based on PTB7-Th and $PC_{71}BM$ via binary solvent additives treatment. Adv Funct Mater 2016;26:6635e40.
[45] Burkhart B, Khlyabich PP, Thompson BC. Influence of the ethylhexyl side-chain content on the open-circuit voltage in rr-poly (3-hexylthiophene-co- 3-(2-ethyl hexyl) thiophene) copolymers. Macromolecules 2012;45:3740e8.